

APPENDIX 5.5.D

CHARACTERIZATION OF WIND LOADING OF TELESCOPES

Published in SPIE Proceedings Vol. 4757, "Integrated Modeling of Telescopes", Lund, Sweden, February 2002, pp72-83.

Characterization of Wind Loading of Telescopes

George Z. Angeli^{1*}, Myung K. Cho¹, Michael Sheehan², Larry M. Stepp¹

¹ New Initiatives Office, AURA Inc., 950 North Cherry Ave., Tucson AZ 85719

² Gemini Observatories, 950 North Cherry Ave., Tucson AZ 85719

ABSTRACT

Ground-based telescopes operate in a turbulent atmosphere that affects the optical path across the aperture by changing both the mirror positions (wind induced vibrations) and the air refraction index. Although the characteristics of the atmosphere are well understood in the inertial range, the validity of the homogeneous, isotropic field assumption is questionable inside the enclosure and in the close vicinity of the structure. To understand the effect of wind on an actual telescope, we conducted extensive wind measurements at the Gemini South Telescope. Simultaneous measurements were made of pressures at multiple points on the mirror surface, as well as wind velocity and direction at several locations inside and outside the dome. During the test we varied the dome position relative to the wind, the telescope elevation angle, the position of windscreens in the observing slit, and the size of the openings in the ventilation gates. The data sets have been processed to provide the temporal and spatial characteristics of the pressure variations on the primary mirror in comparison to the theory of atmospheric turbulence. Our investigation is part of an effort leading to the development of a scalable wind model for large telescope simulations, which describes the forces due to air turbulence on the primary mirror and telescope structure reasonably well even inside an enclosure.

Keywords: wind buffeting, wind model, large telescopes

1. INTRODUCTION

Considering the effects of wind in the design of the next generation giant ground based telescopes is going to be vital to ensure the success of these telescopes. As the sizes of the telescopes are getting larger and larger, the concerns of wind are getting more and more serious. The direct effect of wind is buffeting, i.e. wind inflicted deformations of the mechanical structure as well as the optical elements, like the primary mirror. The primary mirror deformation is especially problematic for large segmented mirrors, where the quality of the optical surface depends only on the stiffness of the back structure and actuators. The severe effect of wind on giant telescopes is aggravated by the fact that the larger the telescope, the lower its resonant frequencies are. Consequently, a larger telescope can absorb a significantly higher percentage of wind energy than a smaller one could.

The same wind also affects local seeing at the telescope through the thermal characteristics of the local turbulence. Extensive studies have proved, that maintaining thermal equilibrium inside the dome can drastically reduce this local seeing. The straightforward way to achieve isothermal surfaces is to allow efficient ventilation of the telescope enclosure. However, the need for ventilation must be balanced against the buffeting effects of the wind.

The behavior of the turbulent atmospheric boundary layer – representing the wind close to the Earth’s surface - is reasonably well understood. The velocity fluctuations at a given point of this turbulent layer may be considered as a superposition of theoretical eddies transported by the mean wind, like a standing wave can be conceptualized as a superposition of traveling waves. Each eddy is assumed to cause a velocity fluctuation at the given point with frequency of f . By analogy to the traveling wave, a wavelength and wave number can be associated with each eddy.

$$\lambda = \frac{U}{f} \quad ; \quad \kappa = \frac{2\pi f}{U} = \frac{\omega}{U}$$

Here U is the mean velocity of the wind. The hypothesis that the “frozen” eddies are traveling with the wind, i.e. the spatial frequency (wavenumber) of turbulence κ is proportional to its temporal frequency f , was first suggested by Taylor (in [1]).

The internal structure of the turbulence layer can be understood as an energy cascading process. When the wind speed u – or more precisely the Reynolds number (Lu/ν) characterizing the airflow - reaches a critical value, the flow becomes turbulent and large eddies appear. However, inside each eddy the speed can still be high enough to generate internal turbulence, i.e. smaller eddies. This cascading goes on until the eddy size L becomes small enough to prevent further turbulence. In the laminar flow then the remaining energy is dissipated as heat.

Kolmogorov's two hypotheses ([2] in [1]) state that there is a range in size of eddies where the fluid motion is locally isotropic and depends only on the rate of energy dissipation ε in the smallest eddies. The boundaries of this inertial subrange are the inner and outer scales (l_0 and L_0 , respectively).

$$\frac{2\pi}{L_0} < \kappa < \frac{2\pi}{l_0}$$

In order to characterize the local structure of turbulence in the atmosphere, Kolmogorov [2] in [1] introduced the structure tensor. After some mathematical and physical considerations ([2] in [1]) [3], [4], [5], the structure tensor yields the one-dimensional structure function, which depends on the scalar distance r and energy transfer rate ε only, with a dimensionless scaling factor of C_u .

$$D_u(r) = C_u \varepsilon^{2/3} r^{2/3}$$

The structure function has a close relationship to the auto-correlation $B_u(0)$ and cross-correlation $B_u(r)$ functions.

$$D_u(r) = 2[B_u(0) - B_u(r)] \quad (1)$$

Bernoulli's Law implies, that - in absence of viscous stresses, - the stochastic properties of the pressure in a given fluid are analogous to those of the square of the velocity. According to Kolmogorov's second hypothesis, in the inertial subrange we can neglect the effect of viscosity. Invoking the same dimensional argument that resulted in the velocity structure function [4], we must consider the dimensions of the velocity square structure function, displacement and energy transfer rate as $(\text{length})^4/(\text{time})^4$, (length) and $(\text{length})^2/(\text{time})^3$, respectively. The resulting structure function has a different scaling factor C_p and steeper distance dependence than the velocity structure function.

$$D_p(r) = C_p \varepsilon^{4/3} r^{4/3}$$

A characteristic length of correlation L_p can be defined for the turbulence by means of the auto-correlation $B_p(0)$ and cross-correlation $B_p(r)$ functions, as an integral scale [6].

$$L_p = \frac{1}{B_p(0)} \int_0^\infty B_p(r) dr$$

Actually the integral can be limited to a bounded region R as long as the cross-correlation is negligible outside of this region. By using the well-known relationship between the structure function and the correlation functions, one can express the integral scale with the structure function only.

$$L_p = R - \frac{1}{D_p(R)} \int_0^R D_p(r) dr \quad (2)$$

According to the Wiener-Khinchine theorem, the power spectral density (PSD) $\Phi_p(\kappa)$ of pressure fluctuation is the Fourier transforms of the cross-correlation function $B_p(\rho)$. Following Tatarski's calculation for velocity power spectral density as an example [4], one can determine the pressure power spectral density in the inertial subrange.

$$\Phi_p(\kappa) = C_p \varepsilon^{2/3} \kappa^{-7/3}$$

However, the power content of eddies certainly does not approach infinity with growing eddy sizes, as the Kolmogorov spectrum implies. Based on experimental results, von Karman suggested power saturation outside the inertial subrange ([7] in [1]). In his formula, the characteristic wave number κ_0 is related to the outer scale of the turbulence, as $\kappa_0 = 2\pi/L_0$.

$$\Phi_p^{vK}(\kappa) = \frac{C_p^{vK}}{\left[1 + \left(\frac{\kappa}{\kappa_0}\right)^2\right]^{7/6}}$$

The temporal power spectral density of the turbulence can be calculated by using Taylor's hypothesis. Here f_0 , the characteristic frequency equals to U/L_0 .

$$\Phi_{pt}^{vK}(f) = \frac{C_{pt}^{vK}}{\left[1 + \left(\frac{f}{f_0}\right)^2\right]^{7/6}} \quad (3)$$

There are several other fitting functions for wind power spectral densities, like Davenport [8], Antoniou [9], Harris [6], etc. but in this work we use the von Karman spectrum for its convenience. Although it is a relatively simple function, it agrees reasonably well with the test results. The von Karman spectrum is fully defined by two parameters, the magnitude C_{pt}^{vK} and the bandwidth f_0 .

Although it is customary to assume a Kolmogorov (or von Karman) spectrum during the design and simulation of telescopes, it is widely considered as a crude estimate only. The turbulence inside the dome is obviously not homogeneous and isotropic enough to support Kolmogorov's hypotheses, certainly not on the scale of the mountaintop environment. To improve the approximation, a frequency dependent multiplying factor, the aerodynamic attenuation was introduced [10], [11]. It is worth to note that people usually choose f_0 and f_a that close to each other.

$$A = \frac{1}{\left[1 + \left(\frac{f}{f_a}\right)^{4/3}\right]^2} \quad (4)$$

The integration of the Gemini South telescope provided an excellent opportunity to conduct extensive wind velocity and pressure measurements in an existing large telescope dome. Besides actual engineering interests – like determining the response of Gemini structure on wind buffeting, or developing a procedure to set the wind gates on that particular enclosure, - our objective was to verify and possibly improve our current understanding of wind loading of telescopes, as well as to work toward a scalable telescope wind model. Some of the results of these measurements were reported earlier [12], [13], [14].

Our particular interest in our investigation resulted in this paper was to find out whether the wind buffeting of the primary mirror was mainly influenced by the outside environment, the enclosure, or local features on and around the mirror. By identifying the source we may get a step closer to actually predicting at least a worst-case wind scenario for telescope designs and simulations.

2. MEASUREMENT SETUP AND DATA REDUCTION

Although during the measurement campaign at Gemini South Telescope a large amount of wind velocity and pressure data was collected, in this work we mainly focus on the pressure distribution measurements on the primary mirror. The details of the data collection were described by Cho *et al.* [12]. Here we repeat only the most relevant information necessary to understand our conclusions.

The measurements were taken inside the Gemini dome, in an environment where the wind was controlled by large wind gates (Figure 1.). At the time of the measurements the glass primary mirror was not installed yet, but there was a steel dummy instead in place. It was covered by plywood to provide a continuous surface. The 32 pressure sensors were installed on this plywood layer according to the configuration shown in Figure 3. The x-axis of the Cartesian coordinate system is parallel to the elevation axis of the telescope with y-axis pointing upward when the telescope is pointed toward the horizon. The actual

environment of the primary mirror is shown in Figure 2. The stray light baffle is clearly noticeable in the picture, together with the mirror cover.



Figure 1. Gemini enclosure with large ventilation gates to allow natural ventilation with ambient air

Data was taken with 16 bit resolution at 10 Hz sampling rate. The total length of each measurement was 5 minutes that resulted in 3000 sampling points. The detection limit (S/N ratio 1) of the pressure sensors is 8 mPa with full range of 20 Pa.

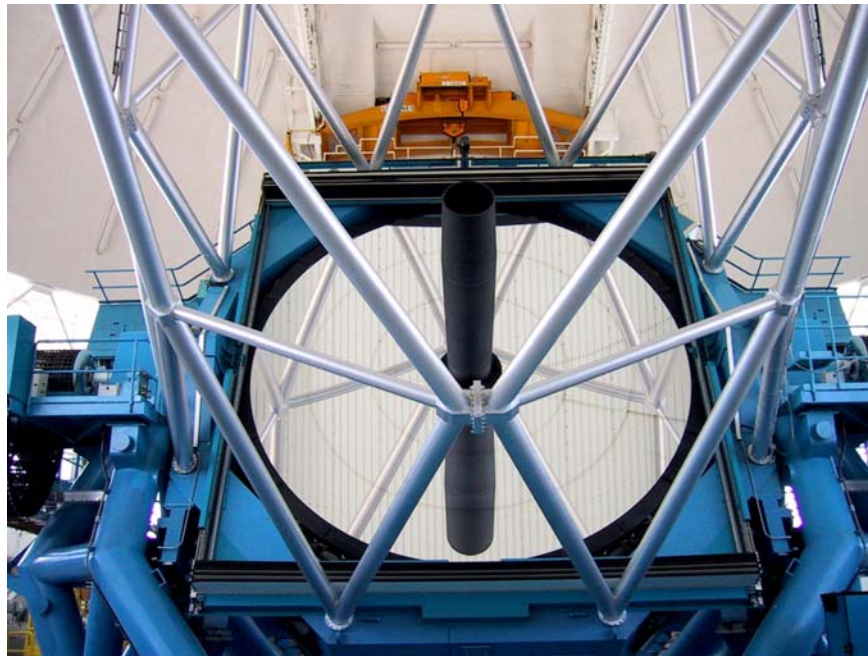


Figure 2. The Gemini primary mirror and its environment

Velocity sensors (three-dimensional ultrasonic anemometers) were also placed at different locations: (i) on the edges of the primary mirror at +X, -X, +Y and -Y positions; (ii) at the secondary mirror; and (iii) on top of the dome. The dome sensor detected the outside wind velocity for reference purposes. In the cases considered in this paper, the ambient wind velocity was ranging from 8m/s to 12 m/s.

The data sets collected have a unique label, for example c090600. The first letter shows the date it was collected, the first three numbers the wind direction and the last two numbers the telescope zenith angle. The tailing two letters indicates the position of ventilation gates: in the example both sides are open. In all cases described in this paper the windshield and shutter are both open leaving the observing slit unobstructed.

The temporal behavior of the turbulence on the primary mirror is characterized by the power spectral densities of the time series collected from each sensor. To estimate the power spectral densities we used Welch’s method [15]. This technique divides the entire time series in sections with length of 256 samples and 50 % overlap, each section is windowed with a Hamming window, and independent periodograms are calculated for each. The final estimate is the average of these periodograms.

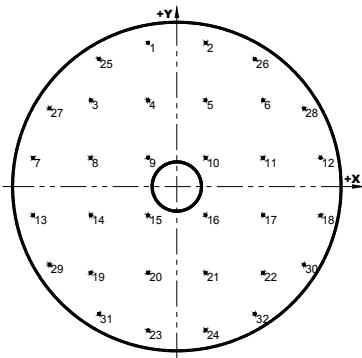


Figure 3. Pressure sensor locations on the dummy primary mirror

To characterize the spatial correlations in the samples, we have used structure functions. Each structure function was directly calculated following the definition by grouping together the sensor pairs with a given distance. Although from a strictly mathematical point of view the structure function is defined on homogenous and isotropic fields, we applied its definition on the turbulent field inside the dome to visualize the analogy and also the differences between inside and outside pressure fields. It should be understood that the structure function averaged over the whole mirror surface is only a global measure of correlation and conceals highly turbulent local effects.

The mean pressure value on the primary mirror is certainly not constant – as it would be expected outside of the enclosure – and is rather deterministic with significant cross-correlation over the whole area. Since our objective was to investigate the random attributes of turbulence, we excluded the mean values from our calculations. Earlier [12], when we were mainly interested in the deformation of the mirror, we reported the structure functions incorporating the mean values.

3. RESULTS

Looking at the pressure power spectral densities, one can recognize evident differences between high and low wind conditions (Figures 4. and 8.). The characteristic differences are clearly recurring, so it’s reasonable to discuss the features of the power spectral densities individually for open and closed ventilation gates.

3.1. Power spectral densities for high winds

When both the windshield and the ventilation gates are open, there is significant wind inside the enclosure. While the mean wind velocity outside the dome is fairly stable, on the edges of the mirror surface it varies widely, depending on the wind direction relative to the dome as well as the zenith angle of the telescope. In the general case, when the wind is blowing on the mirror from an arbitrary direction, the flow field is quite complex and it is rather difficult to identify common patterns. In other words, the local effects of the mirror and mirror support system are seemingly covering up the background turbulence.

Since the detailed velocity distribution on the mirror surface is not available, these local perturbations cannot be extracted from the data to better understand the global (background) effects.

We calculated the pressure power spectral densities for all of the sensors in numerous measurement series detected under various conditions like wind direction and mean velocity, telescope elevation and ventilation gate position. For all tests carried out under high wind conditions, i.e. with open gates, the PSD fits surprisingly well to the theoretical von Karman curve (Equation 3.). The roll-off slope corresponds to the $(-7/3)$ Kolmogorov law with varying bandwidth (f_0) at different areas and under different test conditions (Figure 4.).

To recognize possible patterns, let us consider a relatively simple case, when the telescope is pointing to zenith, i.e. the primary mirror is horizontal, and the wind blows from $(-Y)$ direction (Figures 5. and 6.). In this configuration we can assume a wind velocity and direction that is fairly constant over the mirror surface. Indeed, the anemometers at $(+X)$ and $(-X)$ position detected similar values (3.3 m/s and 3.6 m/s) with similar (close to $+Y$) directions. Even for this setup, the mean pressure on the mirror is far from being constant. However, the RMS pressure plot indicates a noticeable separation between local effects and a more evenly distributed background. It is remarkable that the RMS pressure calculated without considering the mean values is significantly higher than the mean pressure itself, which implies high turbulence.

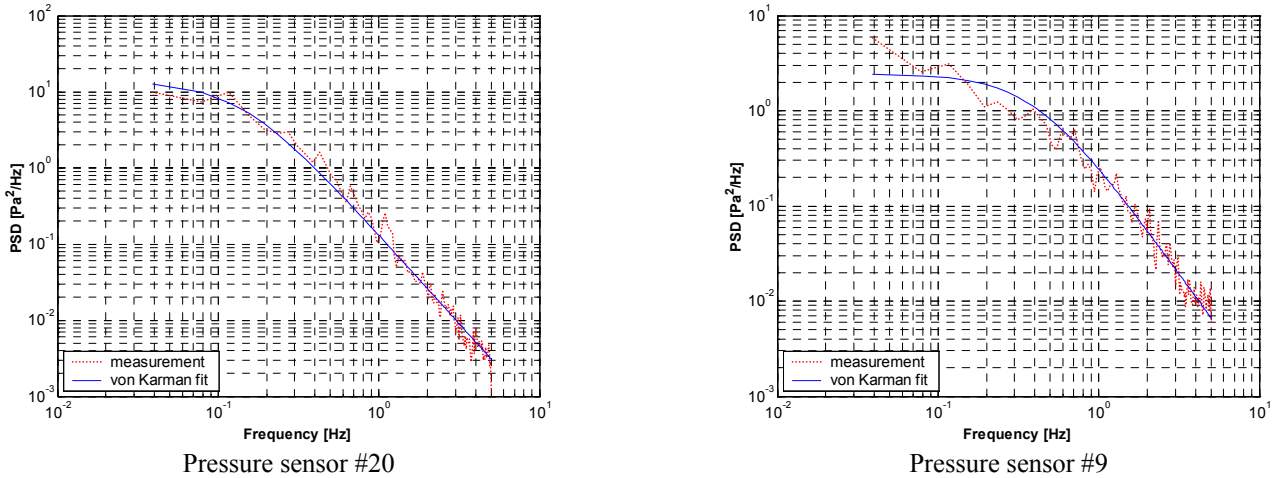
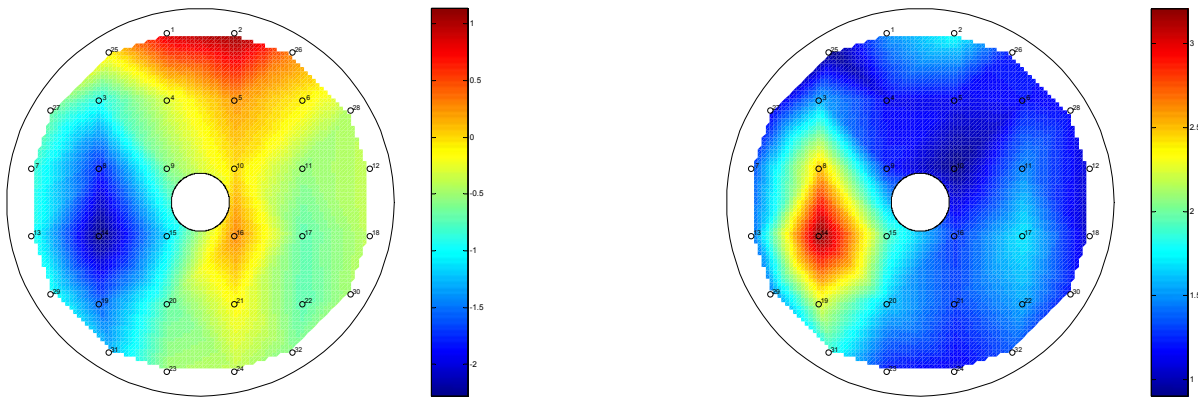


Figure 4. Pressure power spectral densities on the primary mirror with von Karman fit (Data set c00000o).

The turbulence on the mirror can be characterized with the parameters of the curve fit corresponding to Equation 3., i.e. with the magnitude C_{pt}^{vK} and bandwidth f_0 . Indeed, the parameter maps show high energy content without significant turbulence (bandwidth) in the negative pressure area (sensors#8, #14 and #19), which probably indicates a local maximum in tangential wind velocity. On the other hand, there is a highly turbulent area right behind the baffle column, as it appears on the bandwidth plot.

Our assumption is that a characteristic length L_0 - virtually an outer scale - can be derived from the bandwidth f_0 of the background turbulence. This length calculated from the bandwidth average of the background area with the assumption of 3.5 m/s wind speed is about 23 meter. The characteristic length corresponding to the highly turbulent spot behind the baffle is 7.3 meter.

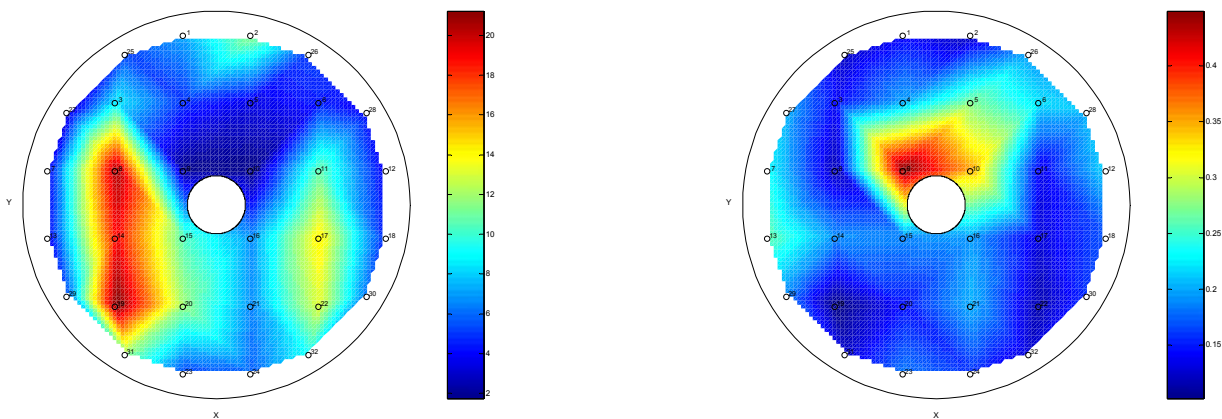
In another case we investigated the telescope zenith angle was 60° with wind blowing sideways, $(-X)$ direction. The mean wind flow was parallel to the mirror surface and reasonably constant, as the anemometers indicated. The gain and bandwidth pattern on the mirror is fairly similar to the horizontal case, except the bandwidth values are significantly higher (Figure 7.) and the pattern is rotated due to the different wind direction. The rotation is less than the expected 90° because the wind is not completely horizontal; it has a slight elevation angle. The bandwidth values are just partly higher due to larger mean velocities (8.5 m/s and 8.2 m/s at $+X$ and $-X$ positions, consecutively). The characteristic length of the turbulence is significantly smaller: the background turbulence corresponds to about 10 meter. The high turbulent area behind the baffle yields a characteristic length of 3.8 meter.



Mean pressure (ranging from -2 to 1 Pa)

RMS pressure (ranging from 1 to 3 Pa)

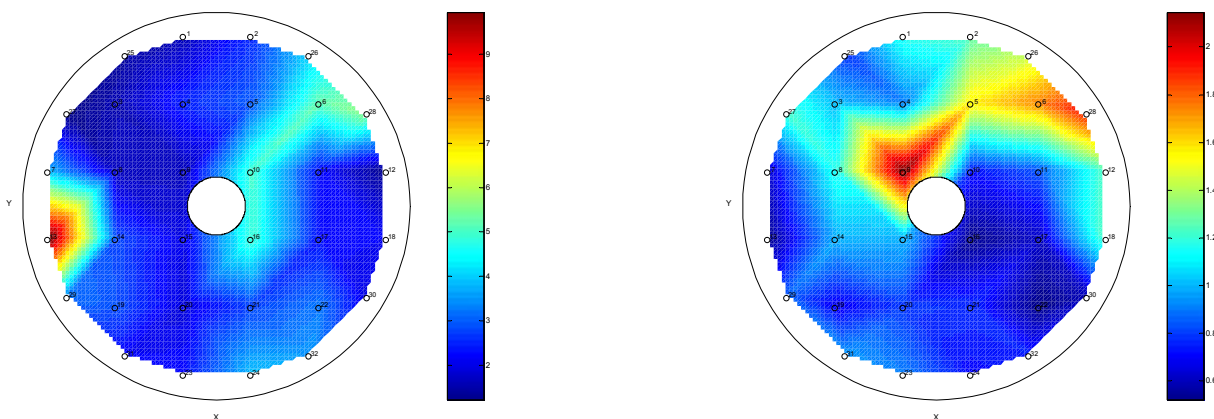
Figure 5. Pressure distribution on the primary mirror pointing to zenith with wind direction of 90° (+Y) (Data set c00000oo)



Magnitude (ranging from 2 to 20 Pa^2/Hz)

Bandwidth (ranging from 0.1 to 0.5 Hz)

Figure 6. Parameters of the best fit for pressure power spectral densities on the primary mirror pointing to zenith with wind direction of 90° (+Y) (Data set c00000oo)



Magnitude (ranging from 2 to 9 Pa^2/Hz)

Bandwidth (ranging from 0.6 to 2 Hz)

Figure 7. Parameters of the best fit for pressure power spectral densities on the primary mirror with zenith angle of 60° and wind direction of approximately 180° (-X) (Data set c09060oo)

Table 1. Characteristic length of background turbulence on primary mirror

$L_0 = \frac{U_{mean}}{f_0}$	ZENITH ANGLE 0° WIND DIRECTION (+Y)		ZENITH ANGLE 60° WIND DIRECTION (-X)	
	L_0	U_{mean}	L_0	U_{mean}
Data set 1 (c00000oo)	23.3 meter	~ 3.5 m/s		
Data set 2 (c09060oo)			10.4 meter	~ 8.3 m/s
Data set 3 (t00000oo)	22.7 meter	~ 5.0 m/s		
Data set 4 (d09060oo)			10.0 meter	~ 10.0 m/s

Other data sets – collected on different days with different mean wind velocities but under similar telescope conditions – yield similar numbers (Table 1.).

3.2. Power spectral densities for low winds

The data collected with closed ventilation gates show some anomaly that needs further investigation. Many sensors detected data with PSD fitting on the Kolmogorov – von Karman curves (Figure 8., sensor #3). However, a significantly high number of sensors – practically the whole right side of the mirror – collected data with much steeper roll-off and a “tail” above 1 Hz (Figure 8., sensor #24). The figure shows a curve fit with von Karman spectrum corrected with the aerodynamic attenuation (Equation 4.). As it is clearly visible in the figure, the fit is not perfect; it estimates fairly well the increased slope, but it does not reflect two major characteristics of the measured curve: (i) the “hump” around 0.2 Hz and (ii) the “tail” above 1 Hz.

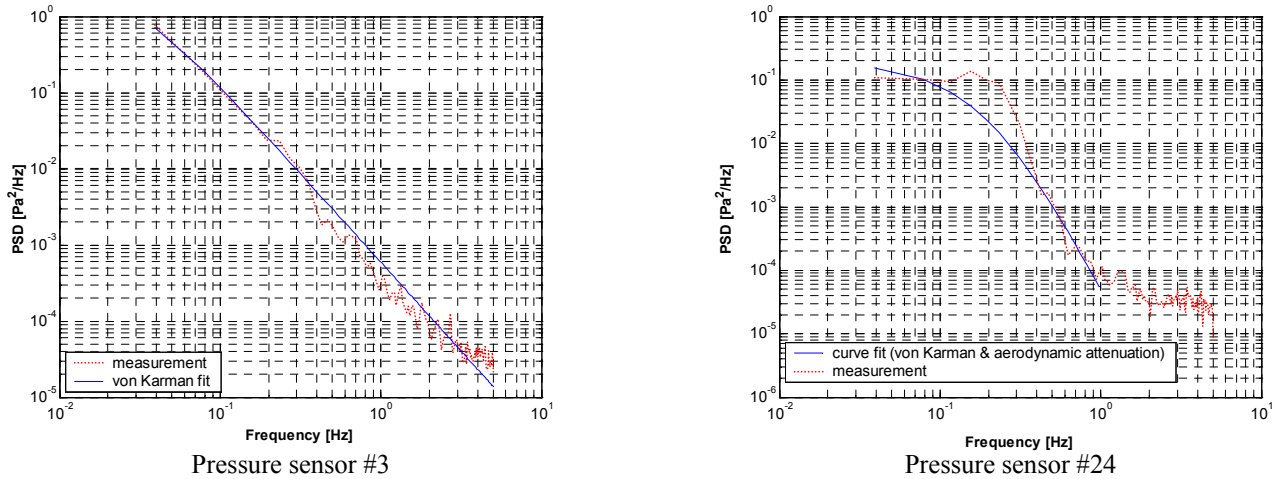


Figure 8. Pressure power spectral densities on the zenith pointing primary mirror with week wind (Data set c00000cc) It is worth to note that the wind speed inside the enclosure was extremely low for this measurement. With the vent gates closed on both sides, the mean wind velocity above the mirror was 0.5 - 1 m/s and the flow field was rather inhomogeneous and complicated.

3.3. Structure function

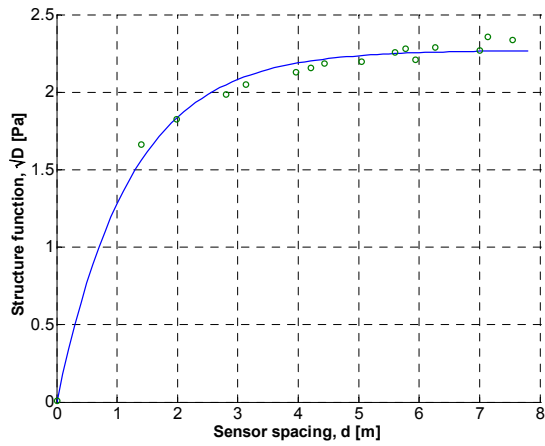
The spatial characteristics of the turbulence can be described with the structure function. To minimize the random effects, the temporal average of the instantaneous structure functions was calculated for the whole 5 minutes collection time. We chose to present the square root of the structure function instead of the structure function itself (Figures 9, 10, and 11), because the

former has a saturation level with the dimension of spatial RMS pressure. Actually, the saturation level is $\sqrt{2}$ times higher than the temporal average of the spatial RMS pressures on the mirror.

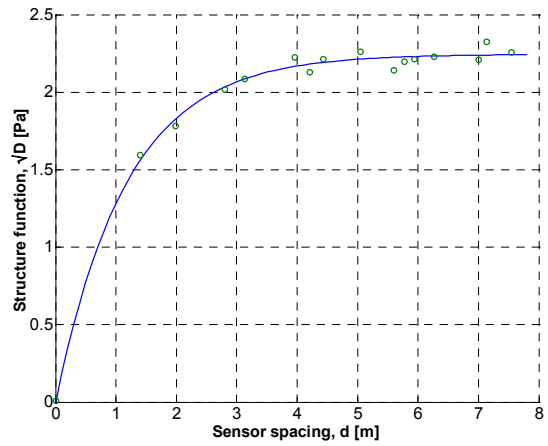
It is obvious from Equation 1. that the structure function saturates as the cross-correlation diminishes with increasing the distance between sensors. It is also obvious from the following definition of the structure function that with zero separation it goes to zero.

$$D_p(r) = \left\langle [p(\mathbf{r}_0 + \mathbf{r}) - p(\mathbf{r}_0)]^2 \right\rangle_{spatial}$$

The correlation length defined in Equation 2. is clearly visible on the plots as “rising distance” of the structure function. The correlation lengths for the different data sets are collected in Table 2. Quite interestingly, the correlation length does not depend on the elevation angle of the telescope, but it shows strong dependence on the azimuth angle. Since the mirror – even with the surrounding telescope structure – seems to be fairly symmetric, it suggests that the correlation length is mainly defined by the environment of the mirror.

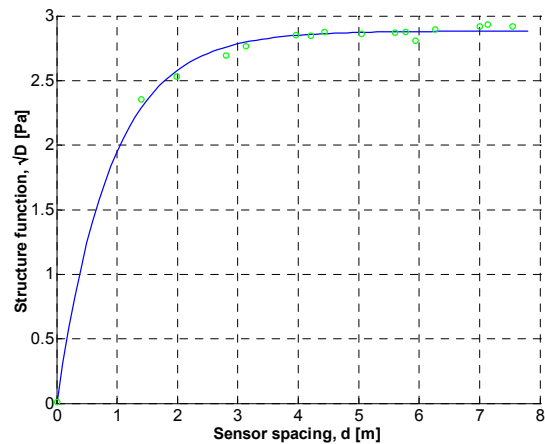


Zenith angle 30° (data set c00030oo)

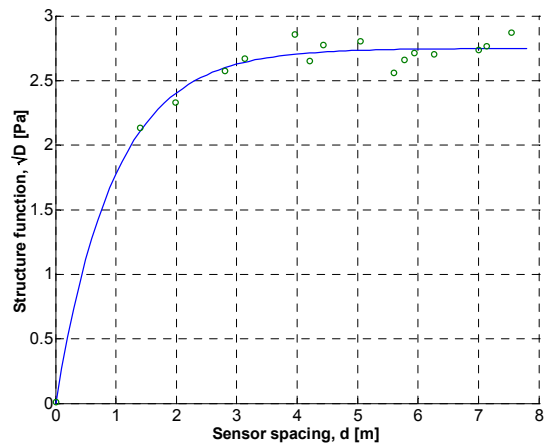


Zenith angle 60° (data set c00060oo)

Figure 9. Pressure structure function on the mirror surface with wind direction of 90° (+Y)

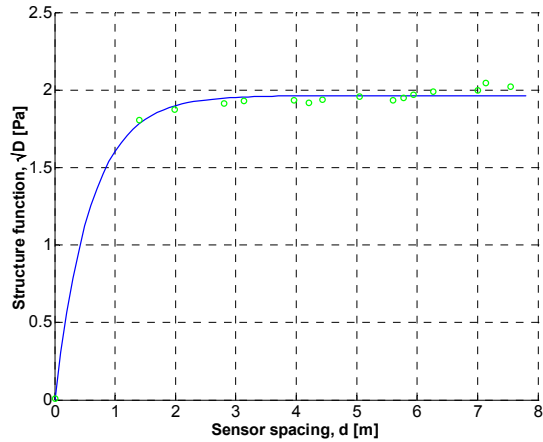


Zenith angle 30° (data set c04530oo)

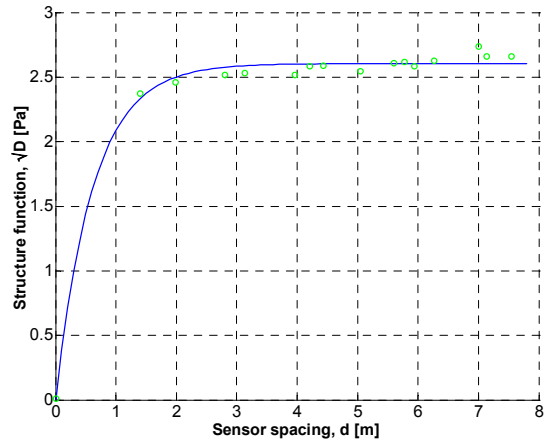


Zenith angle 60° (data set c04560oo)

Figure 10. . Pressure structure function on the mirror surface with wind direction of 135°



Zenith angle 30° (data set c09030oo)



Zenith angle 60° (data set c09060oo)

Figure 11. Pressure structure function on the mirror surface with wind direction of 180° (-X)

According to Simiu [6], the ratio of the characteristic and correlation lengths in turbulence is constant.

$$\frac{L_0}{L_p} = \sqrt{70.8}$$

Where it was possible we derived the correlation lengths of data sets from their characteristic lengths. The results are pretty close to, but slightly higher than the measured values. It is understandable though, considering that the measured structure functions contain the local turbulences that are obviously reducing the correlation, while the bandwidths were calculated only for the background.

Table 2. Correlation length L_p of turbulence on the primary mirror

	WIND DIRECTION 90°		WIND DIRECTION 135°		WIND DIRECTION 180°	
	L_p	data set	L_p	data set	L_p	data set
zenith angle 30°	1.95 meter	c00030oo	1.33 meter	c04530oo	0.83 meter	c09030oo
	1.80 meter	t00030oo	1.71 meter	t04530oo		
zenith angle 60°	1.78 meter	c00060oo	1.38 meter	c04560oo	0.90 meter	c09060oo
	1.88 meter	d00060oo			0.90 meter	d09060oo

4. CONCLUSIONS

It is reasonable to conclude that the background turbulence detected on the mirror is defined by the environment of the mirror, while the local obstacles are causing turbulent effects rather limited in space. Both the power spectral densities and the structure functions indicate that as the wind is moving sideways i.e. its azimuth angle increasing, the airflow above the mirror is getting more turbulent; the bandwidth is increasing while the correlation length is decreasing. Although, as it was reported earlier [12], the overall RMS pressure on the mirror is higher if the mirror is pointing into the wind, the temporal bandwidth of the wind load is rather small. On the other hand, the side wind can cause considerable problems – not because of its intensity but because of its bandwidth. For a telescope of the size of Gemini this wind buffeting frequency is still way below the resonances of the structure, but as telescopes are getting larger, the interaction is more likely.

For single piece primary mirrors – like the Gemini mirror - the correlation length of pressure variations is not a significant feature, since any asymmetric load excites mainly the lowest order structural mode of the mirror, which is astigmatism [12].

However, segmented mirrors are prone to lose their continuity (phasing) if the load is highly uncorrelated, as is the case for side winds in our experiment.

From a control point of view a high bandwidth highly uncorrelated wind load on a segmented primary mirror can pose a substantial challenge. It is worth noting that the correlation length we measured at Gemini is about the size of the mirrors most of the planned extremely large segmented mirror telescopes consider. For these telescopes, either the primary mirror control system, or the enclosure, or rather both should be designed with this fact in mind.

Since any structural element or baffle inside the primary mirror area is likely to generate high bandwidth, local turbulence, the need for them should be carefully balanced. The increased frequency of wind buffeting even on relatively small areas may cause unwanted resonances in extremely large telescopes.

In this paper we considered the cases where we could estimate the wind velocity distribution on the primary mirror from the measurements taken at the edges of the mirror. To separate local and global (background) effects in the general case when the wind blows on the mirror in an arbitrary angle, further investigation is necessary. Computational fluid dynamics (CFD) simulations can predict the velocity distribution above the mirror, which in turn yields the pressure distribution. CFD simulations could also estimate the local turbulence due to obstacles.

ACKNOWLEDGEMENTS

The authors would like to acknowledge the support of the Gemini staff on Cerro Pachon in setting up and performing the wind tests, particularly John Roberts, Gabriel Perez, Pedro Gigoux, Manuel Lazo, and Pablo Prado. We would like to thank Dr. David Smith of MERLAB for organizing the dynamic measurements and collaborating in the data reduction. Special thanks are also extended to Dr. Oleg Likhatchev for his helpful comments and suggestions.

The New Initiatives Office is a partnership between two divisions of the Association of Universities for Research in Astronomy (AURA), Inc.: the National Optical Astronomy Observatory (NOAO) and the Gemini Observatory.

NOAO is operated by AURA under cooperative agreement with the National Science Foundation (NSF).

The Gemini Observatory is operated by AURA under a cooperative agreement with the NSF on behalf of the Gemini partnership: the National Science Foundation (United States), the Particle Physics and Astronomy Research Council (United Kingdom), the National Research Council (Canada), CONICYT (Chile), the Australian Research Council (Australia), CNPq (Brazil) and CONICET (Argentina).

REFERENCES

- [1] S. K. Friedlander and L. Topper, *Turbulence - Classic Papers on Statistical Theory*, (Interscience Publishers, Inc., New York, 1961).
- [2] A. N. Kolmogorov, "The Local Structure of Turbulence in Incompressible Viscous Fluid for Very Large Reynolds Numbers," *Comptes rendus de l'Academie des sciences de l'U. R. S. S.* **30**, 301-305 (1941).
- [3] S. F. Clifford, *Laser Beam Propagation in the Atmosphere*, J. W. Strohbehn, ed., (Springer-Verlag, Berlin, 1978).
- [4] V. I. Tatarski, *Wave Propagation in a Turbulent Medium*, (McGraw-Hill, New York, 1961).
- [5] G. K. Batchelor, *The Theory of Homogeneous Turbulence*, (Cambridge University Press, Cambridge, 1959).
- [6] E. Simiu and R. H. Scanlan, *Wind Effects on Structures - An Introduction to Wind Engineering*, (John Wiley & Sons, Inc., New York, 1986).
- [7] T. von Karman, "Progress in the Statistical Theory of Turbulence," *Journal of Marine Research* **7**, 252-264 (1948).
- [8] A. G. Davenport, "The Spectrum of Horizontal Gustiness Near the Ground in High Winds," *Journal of the Royal Meteorological Society* **87**, 194-211 (1961).
- [9] D. A. Antoniou, "Turbulence Measurements on Top of a Steep Hill," *Journal of Wind Engineering and Industrial Aerodynamics* **39**, 343-355 (1992).
- [10] M. Ravensbergen, "Main Axes Servo Systems of the VLT," *Proceedings of SPIE* **2199**, 997-1005 (1994).

- [11] I. Linares, J. Carlos, and C. Hude, "Overview of the Gran Telescopio Canarias Global Model Simulation," *Proceedings of SPIE* **4004**, 255-266 (2000).
- [12] Cho, Myung, Stepp, Larry and Kim, Seongho. , "Wind Buffeting Effects on the Gemini 8m Primary Mirrors," *Proceedings of SPIE* **4444**, 302-314 (2001).
- [13] Smith, David, Weech, Keith, Teutsch, Johann, Avitabile, Peter, Gwaltney, Geoff, Sheehan, Mike, and Cho, Myung. Comparison of Pressure Measurements and Operating Data for Wind Excitation of Telescope Structures. 2001. Proceedings of the 19th International Modal Analysis Conference. Kissimmee, FL
- [14] Avitabile, Peter, Weech, Keith, Smith, David, Gwaltney, Geoff, and Sheehan, Mike. Modal and Operating Characterization of an Optical Telescope. 2001. Proceedings of the 19th International Modal Analysis Conference. Kissimmee, FL
- [15] *Signal Processing Toolbox User's Guide*, (The MathWorks, Inc., 2001).